Skyrmion stability in nanocontact spin-transfer oscillators

C. P. Chui[1] and Yan Zhou[1,2,a]

[1]*Department of Physics, the University of Hong Kong, Pokfulam, Hong Kong*
[2]*York-Nanjing Joint Center for Spintronics and Nano Engineering (YNJC), School of Electronic Science and Engineering and Collaborative Innovation Center of Advanced Microstructures, Nanjing University, Nanjing 210093, China*

We investigate the conditions for nanocontact spin-transfer oscillators (NC-STOs) that allow for stabilization of a skyrmion. Emphasis is made on the breathing mode, which can be regarded as a source of microwave generation. Micromagnetic simulations of NC-STOs with varying parameters have been performed, with the resulting magnetization plotted in the form of phase diagrams. It is found that control of spin wave mode in conventional STOs can be applied to skyrmion-based STOs. © *2015 Author(s). All article content, except where otherwise noted, is licensed under a Creative Commons Attribution 3.0 Unported License.* [http://dx.doi.org/10.1063/1.4930904]

I. INTRODUCTION

The ability of magnetic nanostructures to generate microwave has been discovered experimentally.[1] The major types of such nanostructures are nanopillars and nanocontact spin-transfer oscillators (NC-STOs). The advantages of NC-STOs compared to nanopillars include narrow linewidth of MHz order and a higher quality factor up to 18,000.[2]

Due to lower Joule heating by using a lower current density,[3,4] possibilities of skyrmions as information storage units and microwave generators have been widely investigated in recent years. For example, theoretical analysis has been performed as to the skyrmion stability in a magnetic nanodot,[5] suggesting that the aspect ratio of the nanodot controls the suitable perpendicular magnetic anisotropy (PMA) of the material, which facilitates the stability of skyrmions in the absence of the Dzyaloshinskii–Moriya interaction[6,7] (DMI). In addition, attempt has recently been made on multiple skyrmions in an NC-STO, indicating that their orbit around the nanocontact is potentially useful for microwave frequency generation.[8]

In formulating skyrmion-based NC-STOs, reference to studies of conventional STOs (*e.g.* Refs. 9–11) is necessary. These studies involve the design of the fixed layer, the spacer, and the free layer of an STO, as well as the appropriate combination of current density and magnetic field.

The effect of polarization angle on the fixed layer of NC-STOs has been studied. For conventional STOs, it is found that some angles of polarization are beneficial to microwave frequency generation by magnetization precession in the absence of external magnetic field.[9] The resulting phase diagram also demonstrates a variety of static and dynamic states in the absence of an external magnetic field.[10] However, the effect of tilting the polarization angle on skyrmion stability is lacking in the literature.

The in-plane torque and field-like torque determine the current-induced magnetization dynamics. It is known that the in-plane torque counteracts the damping of magnetization. On the other hand, the role of the field-like torque in conventional STOs is yet to be clarified.[11] Furthermore, the role of both torques in stabilizing a skyrmion is seldom discussed as well.

The exchange field controls the rate of both precession and damping of the magnetization. The importance of exchange field in stabilizing a skyrmion in ferromagnetic thin films has been

[a]Correspondence and requests for materials should be addressed to Yan Zhou (yanzhou@hku.hk).

5, 097126-1

discussed.[12,13] To our knowledge, however, the extent of the exchange field to a skyrmion in an NC-STO has not been investigated.

It is known that the nanocontact radius controls the spin wave mode. It is found theoretically that the excited spin wave mode is a function of the nanocontact radius.[14] Both micromagnetic simulations and experimental work have verified this idea later on.[15,16] The excitation mode of a skyrmion residing in an STO should be expected to be adjustable by the nanocontact dimensions.

The control of an NC-STO by means of varying the applied magnetic field and direct current has been achieved, which becomes an important mechanism to tune the spin wave mode for the desired operating frequency. For example, experimental results indicate that the operating frequency of an STO increases with the field strength and decreases with the injected current density.[17] As another example, a magnetic field directed at some oblique angle can result in a higher precession frequency of an NC-STO.[18] It has also been realized that specific angles of the magnetic field can change the spin wave in an NC-STO between the bullet mode and the propagating mode.[19] Whether the same phenomenon can be obtained for skyrmion-based STOs is of interest to magnetic device designers.

Spin transfer oscillators based on magnetic vortices have been extensively studied experimentally and numerically.[20–23] Oscillators based on magnetic vortices have been found to exhibit a narrow linewidth.[24,25] Skyrmion in NC-STOs is thus a promising candidate of microwave generation and spin wave based computing and logic.

We propose some criteria for ensuring the stability of a skyrmion in an NC-STO. A number of fine tunings as have been performed on conventional NC-STOs are attempted in the skyrmion-based NC-STOs to determine the interplay among the parameters which constitute the favorable conditions of storing a skyrmion. The results are presented by means of magnetic phase diagrams. By comparing with conventional NC-STOs, we suggest the similarities and differences of skyrmion-based NC-STOs.

This article is organized as follows. Section II describes the micromagnetic approach to evaluating the magnetization of the free layer. Section III portrays a number of phase diagrams obtained from tuning the material and external parameters of the an STO. Section IV is a discussion section about the suggested parameters that facilitate the stabilization of a static skyrmion and a breathing skyrmion. Section V is the conclusion of the article.

II. METHODS

MuMax3,[26] an open-source tool of micromagnetic simulations running in graphics processing units (GPU), has been used in this study. The simulation relies on the numerical solutions to the Landau-Lifshitz-Gilbert-Slonczewski (LLGS) equation, which governs the dynamics of magnetization in the free layer caused by the spin-polarized current. The partial differential equation of the motion of free-layer magnetization $\mathbf{m}$ with respect to time t is written as[26]

$$\frac{\partial \mathbf{m}}{\partial t} = \frac{\gamma}{1 + \alpha^2} \left\{ \mathbf{m} \times \mathbf{B}_{\text{eff}} + \alpha \left[\mathbf{m} \times (\mathbf{m} \times \mathbf{B}_{\text{eff}}) \right] \right\}$$
$$+ C \frac{\epsilon - \alpha \epsilon'}{1 + \alpha^2} \left[\mathbf{m} \times (\mathbf{m}_{\text{p}} \times \mathbf{m}) \right] - C \frac{\epsilon' - \alpha \epsilon}{1 + \alpha^2} \left(\mathbf{m} \times \mathbf{m}_{\text{p}} \right), \tag{1}$$

$$C = \frac{J_z \hbar}{M_{\text{sat}} e l}, \tag{2}$$

$$\epsilon = \frac{P \Lambda^2}{(\Lambda^2 + 1) + (\Lambda^2 - 1)(\mathbf{m} \cdot \mathbf{m}_{\text{p}})}. \tag{3}$$

Here, γ is the gyromagnetic ratio, α is the Gilbert damping constant, $\mathbf{B}_{\text{eff}}$ is the effective magnetic field, $\mathbf{m}_{\text{p}}$ is the magnetization of the polarizer or the fixed layer, J_z is the current density in the z-direction, M_{sat} is the saturation magnetization, e is the electronic charge, l is the thickness of the free layer, $\hbar$ is the reduced Planck constant, and P is the spin polarization. $\Lambda = (RG)^{1/2}$ is the Slonczewski asymmetry parameter which consists of two parts.[27,28] The first part is the spin effective resistance R between the NC lead and the spacer, whereas the second part is the conductance

G between the ferromagnetic layer (either free or fixed layer) and the spacer. ϵ characterizes the strength of the in-plane component of the spin transfer torque (*i.e.* in-plane torque), whereas ϵ' is the secondary spin transfer torque (STT) parameter that accounts for the strength of the out-of-plane component of the spin transfer torque (*i.e.* field-like torque).[29] Usually, $\Lambda = 1$ in symmetric systems, in which two NC leads are identical and two ferromagnetic layers (fixed and free) are identical. The effective field is the vector sum of the demagnetizing field $\mathbf{B}_{demag}$, the exchange field $\mathbf{B}_{exch}$, the anisotropy field $\mathbf{B}_{anis}$, as well as the external field $\mathbf{B}_{ext}$. It is noted that the current density J_z is defined as positive when the electrons are directed from the fixed layer to the free layer.

A skyrmion of downward polarity and counter-clockwise chirality has been placed as the initial condition of the free layer magnetization. The Dormand-Prince solver has been applied to solve the LLGS equation. The size of discretization cells employed for each NC-STO is between 1 nm and 2 nm. All NC-STOs have been simulated for 10 ns. Variable time steps of around 1 fs have been implemented in solving Eq. (1).

Fig. 1(a) depicts the setup of an oscillator in cylindrical geometry. The bottom layer is the polarizer, the middle layer is the spacer, and the top one is the free layer. The two smaller cylinders at the top and the bottom represent the NC leads. The angle between $\mathbf{m}_p$ and the fixed layer plane is denoted by β. The free layer has diameter denoted by d_{layer}. As Fig. 1(a) shows, J_z is positive when the conventional current passes through the free layer followed by the fixed layer. The nanocontact radius is denoted by $d_{contact}$. The polar angle of the external magnetic field is θ.

The default parameters for Pt|Co based NC-STOs are listed as follows.[30] The free layer thickness l is 1 nm. $K_u = 0.8$ MJ/m^3 is the first-order uniaxial anisotropy constant, $D_{ind} = 3$ mJ/m^2 is the interfacial DMI, $M_{sat} = 580$ kA/m is the saturation magnetization, $A_{ex} = 15$ pJ/m is the exchange stiffness, and $\alpha = 0.3$ is the damping constant. The Slonczewski asymmetry parameter $\Lambda = 1$, and the secondary spin transfer torque parameter $\epsilon' = 0$. The nanocontact diameter is 50 nm, wherease the free layer diameter is 200 nm. The polarization angle β is set to be 90°, meaning that it is perpendicular to the fixed layer. The current density J_z is set at -3×10^8 A/cm^2, so the electrons
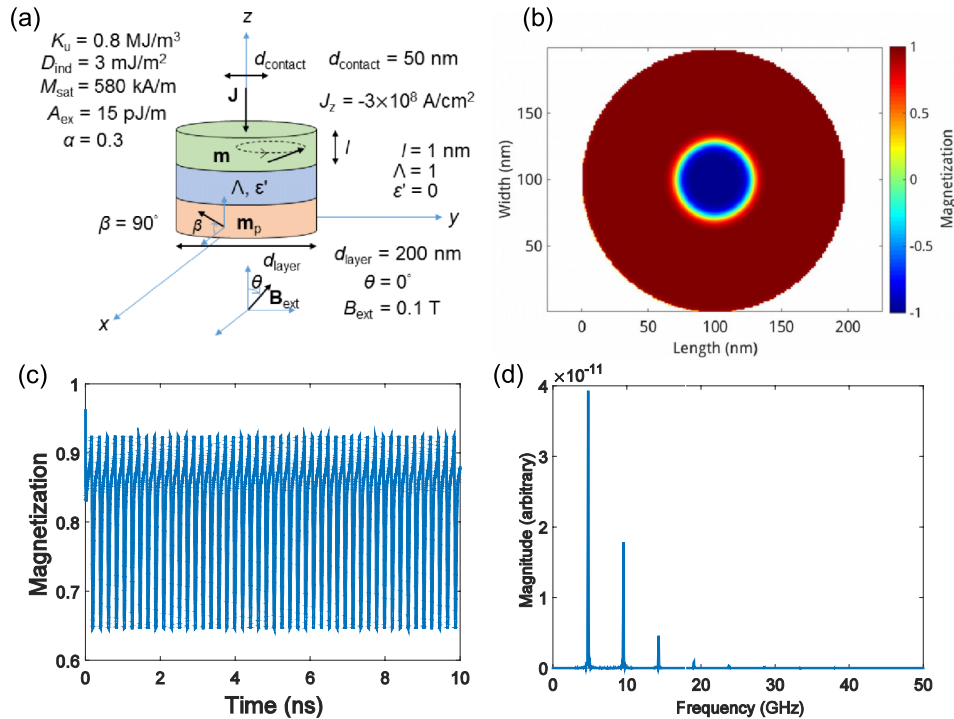

FIG. 1. (a) The schematic setup of an NC-STO. (b) The corresponding m_z plot of Fig. 1(a) for the simulation time of 10 ns. The color bar represents the scale of m_z. The free layer magnetization is obtained after the electrons are reflected by the fixed layer. (c) The evolution of m_z. (d) The frequency spectrum of m_z obtained for the 10-ns simulation.

enter the fixed layer first. The external field is directed at $\theta = 0\,°$, meaning that it is perpendicular to the free layer. The applied field strength $B_{ext} = 0.1$ T.

For easier comparison in the following sections, the out-of-plane magnetization m_z of the NC-STO is plotted in Fig. 1(b). It is clear that a skyrmion can be stabilized after 10 ns. The time traces of the average z-component of the magnetization *i.e.* m_z of the free layer is shown in Fig. 1(c). The frequency spectrum of m_z by means of the Lomb-Scargle method targeted at variable time steps is shown in Fig. 1(d). One can realize that the skyrmion is in breathing mode, whose fundamental frequency is about 5 GHz. A number of harmonics also exists in the frequency spectrum, indicating the nonlinearity of such breathing mode of the STO. The rest of the article focuses on the change of the magnetic phases of the STOs from the default one, with other material and external parameters being varied.

In the Results section (Section III), all the parameters except those two to be tuned in separate phase diagrams will remain unchanged as those in Fig. 1(a). Besides, the breathing rate of a skyrmion is determined by the frequency of the largest power obtained by the Lomb-Scargle periodogram, which can sometimes be a higher harmonic instead of the fundamental frequency. Many of the NC-STOs simulated can exhibit noticeable modulation of m_z rather than m_x and m_y, so the breathing frequency is obtained from the frequency spectrum of m_z.

III. RESULTS

We start with the phase diagrams involving the parameters pertaining to the fixer layer, followed by those pertaining to the space and to the free layer. Phase diagrams as functions of external parameters are displayed in the final subsection.

A. Tuning the fixed layer

First, we investigate the $J_z - \beta$ phase diagram, where $0° \leq \beta \leq 90°$ and -5×10^8 A/cm^2 $\leq J_z \leq +5 \times 10^8$ A/cm^2. In Fig. 2(a), the $J_z - \beta$ phase diagram is composed of snapshots of the magnetization at 10 ns. It indicates that the spin-polarized current can change the circular nature of the initial skyrmion when the polarization deviates from the vertical direction (e.g. $\beta = 85°$).

Initially the breathing mode is realized under the out-of-plane alternating magnetic field.[31] However, this mode can be achieved by a constant magnetic field according to our study. The main frequencies of the breathing mode under varying β and J_z are recorded in Fig. 2(b). We can
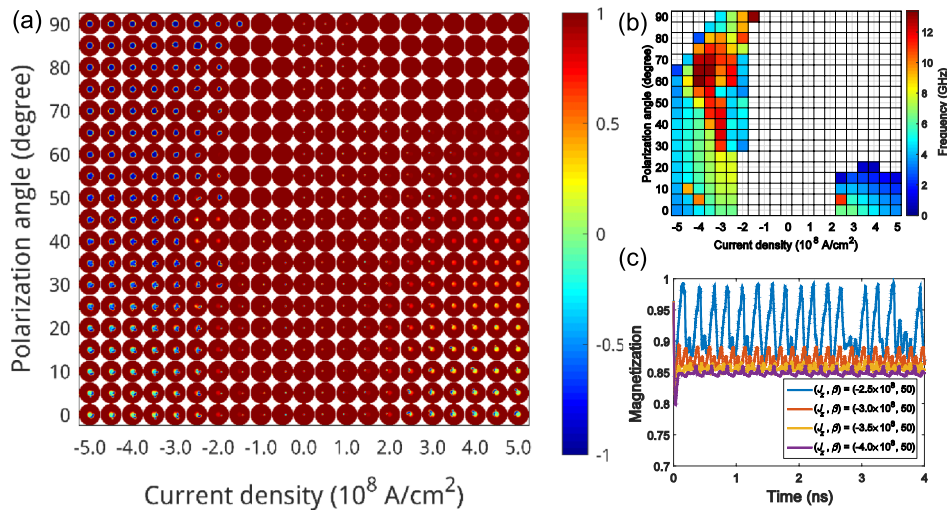

FIG. 2. (a) Snapshots of the $J_z - \beta$ phases of NC-STOs at 10 ns. The color bar indicates the m_z value of the STOs. (b) The frequency of breathing for the range of parameters used in (a). (c) The temporal variation of m_z for four STOs after 4 ns of simulation time, indicating the highly non-sinusoidal waveform of m_z.

realize that the resulting magnetization for all tilt angles has a finite frequency of GHz order. The trend of the frequency of breathing is not apparent because the time-varying m_z waveform is highly non-sinusoidal (as indicated by the m_z waveform with time in Fig. 2(c)). It is inferred that the phase region with higher frequencies have a number of higher harmonics. It is therefore more difficult to identify the most representative frequency of an STO in this case.

B. Tuning the spacer

Here we obtain the magnetization of NC-STOs by choosing $0.1 \leq \Lambda \leq 2$ and $0 \leq \epsilon' \leq 0.2$. The snapshots of the $\Lambda - \epsilon'$ phase diagram at 10 ns can be found in Fig. 3(a). According to our findings, these two parameters allow a wider choice for the mere maintenance of a skyrmion. It is known that the field-like torque is insignificant in spin valves,[32] so the effect of ϵ' is minimal. Fig. 3(a) seems to agree with the result in the literature, in which a skyrmion can be stabilized except ϵ' is particularly small ($\epsilon' < 0.08$). For Λ, as long as it is above 0.5, a skyrmion can be stabilized. It implies that asymmetric systems can permit the formation of a skyrmion.

While skyrmions can be formed easily in a wide range of the $\Lambda - \epsilon'$ combination, only a small portion of them can generate frequency by breathing. In Fig. 3(b), only those NC-STOs where $\Lambda \in [0.2, 1]$ and $\epsilon' \in [0, 0.09]$ allows skyrmion breathing. Moreover, the variation of the breathing frequency as a result of varying Λ and ϵ' is generally insignificant. There are some points of particularly high frequency in Fig. 3(b) at $\Lambda = 0.4$, because these points arise from the highly non-sinusoidal magnetization waveform. Fig. 3(c) shows some of these waveforms at $\Lambda = 0.4$, which possibly indicate the metastable state between the static/breathing state as Λ increases.

C. Tuning the free layer

In order to study the effect of the exchange field on a skyrmion in an NC-STO, we tune M_{sat} and A_{ex} such that 50 kA/m $\leq M_{sat} \leq$ 1,000 kA/m and 1 pJ/m $\leq A_{ex} \leq$ 20 pJ/m. The $M_{sat} - A_{ex}$ phase diagram at 10 ns is shown in Fig. 4(a), which indicates that there exists a lower limit of A_{ex} that can sustain a skyrmion. If A_{ex} is too small, the magnetization of a large number of NC-STOs becomes the form of a chiral liquid.

Fig. 4(b) compares the frequency of NC-STOs with the largest power when M_{sat} and A_{ex} are varied, most of which is the fundamental frequency. While a large number of NC-STOs in the given
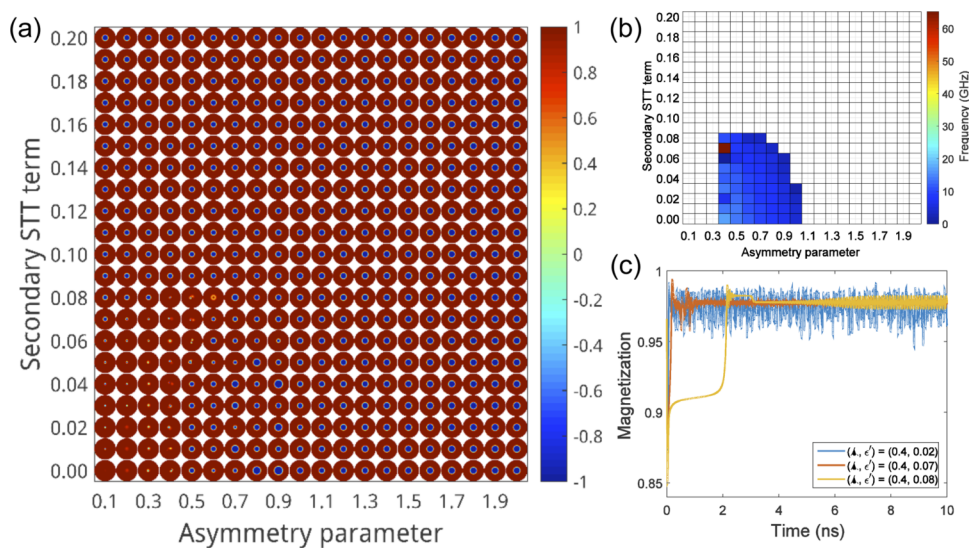

FIG. 3. (a) Snapshots of the $\Lambda - \epsilon'$ phase at 10 ns. The color bar is the m_z scale of the STOs. (b) The frequency of breathing for the range of parameters used in (a). (c) The temporal variation of m_z for three STOs, demonstrating the instability of breathing at $\Lambda = 0.4$.
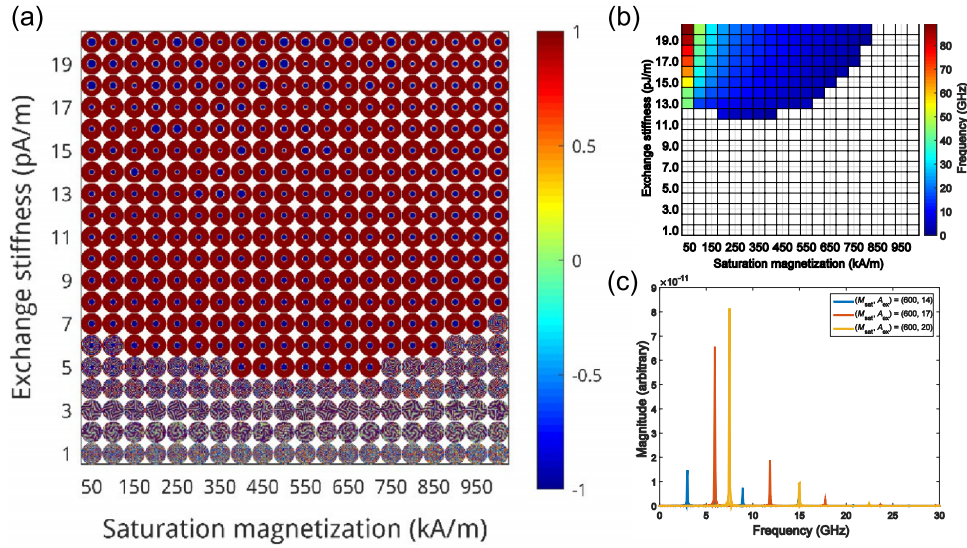
FIG. 4. (a) The $M_{sat} - A_{ex}$ phase diagram composed of the snapshots at 10 ns. The m_z value of the STOs are shown on the color bar. (b) The frequency plot of the STOs attempted, with the highest frequencies occurring at extremely low M_{sat}. (c) The frequency spectra of three STOs obtained from m_z, indicating the decrease in the power of higher harmonics with the fundamental frequency as M_{sat} is kept constant.

M_{sat} and A_{ex} ranges can sustain a skyrmion, only those with smaller M_{sat} and larger A_{ex} can allow for breathing. The breathing frequency increases with A_{ex}, while it decreases with M_{sat}. It is deduced that materials with large M_{sat} require large A_{ex} to stabilize a breathing skyrmion. Except those NC-STOs with extremely low M_{sat}, whose frequency can be over 80 GHz, the breathing frequency within the given M_{sat} and A_{ex} range is below 20 GHz. According to Fig. 4(c), higher harmonics are more suppressed as the fundamental frequency increase, which can be achieved by a larger A_{ex} while keeping M_{sat} fixed.

The snapshots of the $D_{ind} - K_u$ phases at 10 ns are presented in Fig. 5(a). We generate the phase diagram by setting $0 \text{ mJ/m}^2 \leq D_{ind} \leq 9 \text{ mJ/m}^2$ and $0 \text{ MJ/m}^3 \leq K_u \leq 2 \text{ MJ/m}^3$. One can find
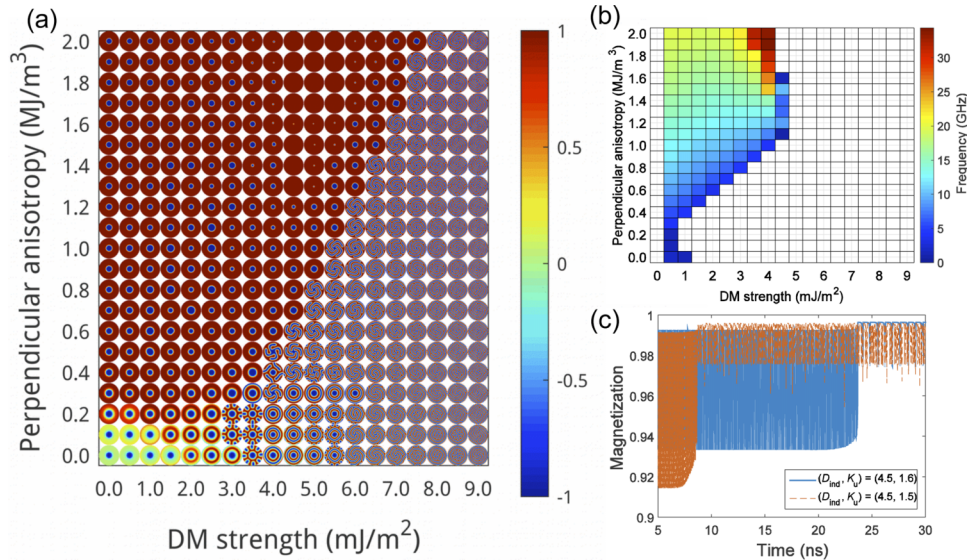

FIG. 5. (a) The $D_{ind} - K_u$ phase diagram composed of the snapshots at 10 ns. The color scale of m_z shown in the phase diagram is given on the right. (b) The main frequency of the STOs. (c) The m_z plots of two STOs with $(D_{ind}, K_u) = (4.5, 1.5)$ and $(D_{ind}, K_u) = (4.5, 1.6)$ near the static/breathing boundary, which demonstrate an abrupt change of m_z amplitude and frequency after some time.

some similarities to the case in a magnetic nanowire.[33] In general, skyrmions can be stabilized at a higher DMI and a larger PMA. For a low DMI and a low PMA, the core of a skyrmion can remain unchanged while the area outside the nanocontact has turned to in-plane magnetization. The result indicates that the magnetization underneath the NC is controlled by the spin-polarized current. As another implication, the winding of magnetization relies largely on the DMI when the PMA is small. An external magnetic field and a spin-polarized current alone cannot warrant the maintenance of a skyrmion. For an even larger DMI, a skyrmion would end up with a completely distorted magnetization, which can no longer be rectified by increasing the PMA.

The frequencies of the breathing mode accompanying the $D_{ind} - K_u$ phase diagram can be found in Fig. 5(b), which shows the main frequencies when the simulation time approaches 10 ns. The frequency of breathing is approximately between 1 GHz and 35 GHz. In general, the breathing frequency increases with PMA for a wide range of DMI. Another property of the frequency spectra arising from these NC-STOs is that they resemble the default one in Fig. 1(d), which has the largest power at the fundamental frequency.

The time instant of recording the frequency is important in the $D_{ind} - K_u$ phase diagram because it is found that the frequency of breathing and the amplitude of m_z fluctuation might vary after 10 ns. For further investigation, we perform the simulation of particular STOs for a longer simulation time. For example, Fig. 5(c) indicates that the frequency changes after 9 ns for $(D_{ind}, K_u) = (4.5, 1.5)$ and after 24 ns for $(D_{ind}, K_u) = (4.5, 1.6)$, respectively. It suggests that a large DMI at a large PMA that allows for a breathing skyrmion can result in unstable frequency output of an NC-STO. Besides, the amplitude of m_z variation is narrowed as D_{ind} increases. This means that the breathing mode of a skyrmion decays with increasing D_{ind}. The skyrmion would revert to a static one in the DMI is further increased. As both PMA and DMI approach the static/breathing phase boundary, (*i.e.* the red region of Fig. 5(b)), the breathing frequency becomes significantly higher due to this instability of frequency. The increased frequency at the static/breathing phase boundary (as the red dots in Fig. 5(b) demonstrate) can thus be referred to as the metastable state between these two states.

The $d_{contact} - d_{layer}$ phase diagram is shown in Fig. 6(a), with condition $d_{contact} \leq d_{layer}$. Here, $d_{contact}$ ranges from 20 nm to 200 nm, whereas d_{layer} ranges from 50 nm to 500 nm. A large proportion of the NC-STOs can stabilize the skyrmion state after 10 ns, with the skyrmion core area increasing with the NC area in general. It implies that the NC area controls the core size of a skyrmion. As $d_{contact}$ increases while keeping d_{layer} fixed, a complete winding of magnetization has to be performed at the remaining area between the NC and the rim of the free layer.
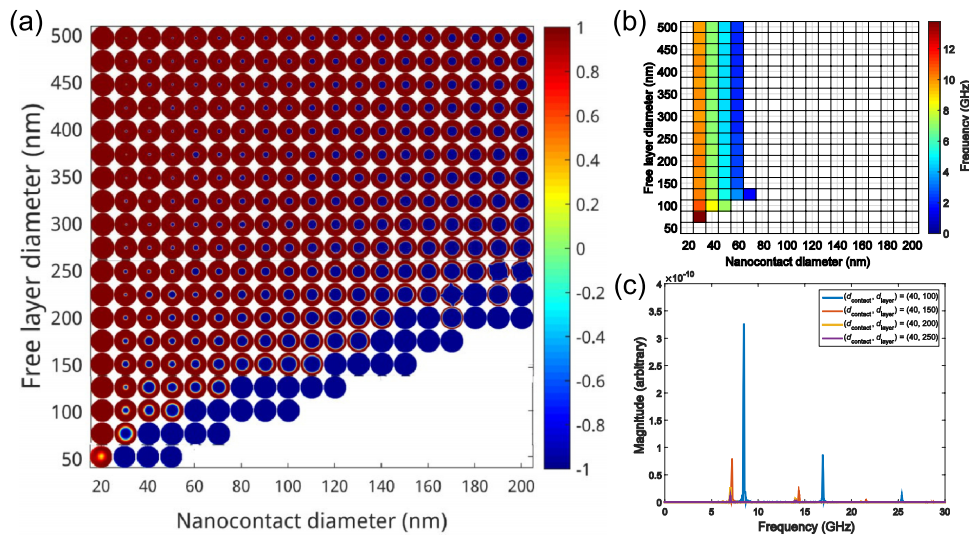

FIG. 6. (a) The $d_{contact} - d_{layer}$ phase diagram composed of the snapshots at 10 ns. The m_z scale is shown on the color bar. (b) The main frequency of the STOs. (c) The frequency spectra of m_z for four phase points (40, 100), (40, 150), (40, 200), and (40, 250), showing the minimal effect on the fundamental frequency with the increase in the nanocontact diameter, at least numerically.

As shown in Fig. 6(b), a majority of the skyrmions simulated are in static mode, whereas a minority of them are in breathing mode. The breathing mode can be obtained as $d_{contact}$ is approximately between 30 nm and 60 nm, with no special restriction on d_{layer}. In addition, if d_{layer} is not exceptionally close to $d_{contact}$, the breathing frequency is nearly independent of d_{layer} for a given $d_{contact}$, at least numerically. Consistently, the higher harmonics are nearly unchanged with d_{layer} after $d_{contact}$ is fixed. Fig. 6(c) displays a number of frequency spectra, in which $d_{contact}$ is fixed at 40 nm and d_{layer} are between 100 nm and 250 nm. It is noted that the frequency spectra for $(d_{contact}, d_{layer}) = (40, 200)$ and $(d_{contact}, d_{layer}) = (40, 250)$ almost overlap each other, which demonstrates that further increasing $d_{contact}$ has an insignificant effect of the frequency and even the power of the higher harmonics.

The case with $d_{contact} = d_{layer}$ can be referred to as a nanopillar. For example, the phase points $(d_{contact}, d_{layer}) = (100, 100)$ and $(d_{contact}, d_{layer}) = (200, 200)$ in Fig. 6(a) indicate that an initial skyrmion is evolved to an entirely spin-down state. This phenomenon is consistent with our findings that the skyrmion core increases with the NC area.

A number of theoretical and numerical studies, *e.g.* Refs. 34 and 35, have indicated that the spin wave mode in a conventional STO is determined by the threshold current I_{th} injected through the nanocontact toward the free layer. The threshold current is a function of the nanocontact dimensions as well as the parameters of the free layer underneath the nanocontact. The threshold current is independent of the diameter of the entire free layer, so once the nanocontact diameter is fixed we do not find a change in operating frequency from a larger free layer diameter.

When the current density is fixed and the nanocontact has a larger diameter (above 70 nm in our simulation), the current passing through the free layer is also larger. At such a larger current, the static skyrmion mode is induced.

We end this section by demonstrating the role of damping on skyrmion stability. Fig. 7 shows the effect of using a damping constant α smaller than 0.3. This figure is calculated by changing α while maintaining other parameters listed in the schematic setup (Fig. 1(a)) unchanged. As shown
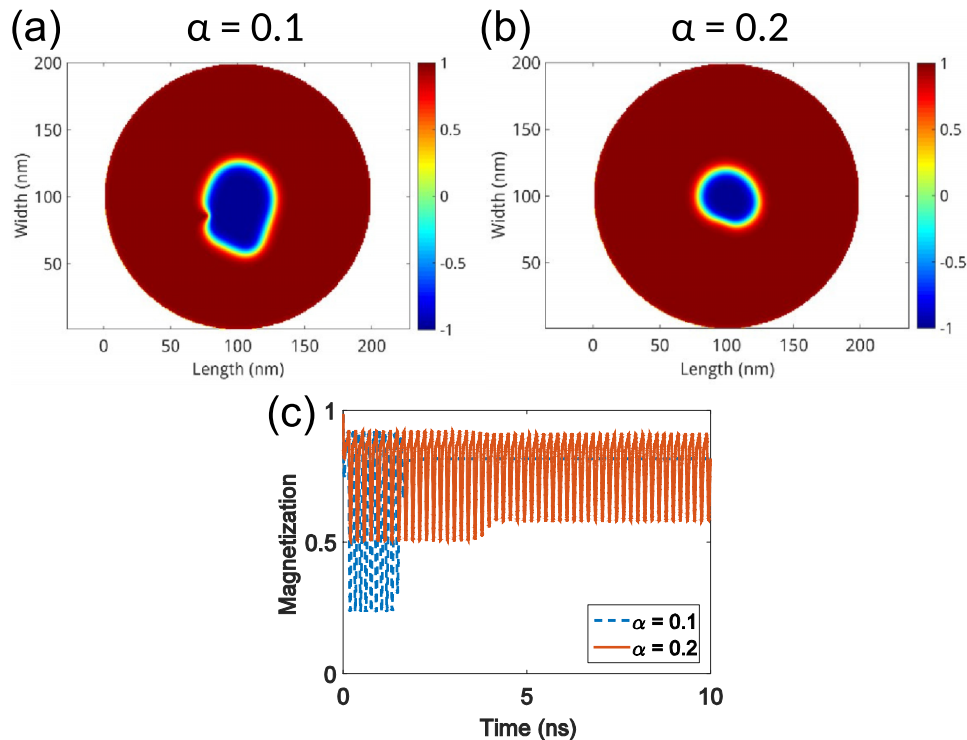

FIG. 7. The magnetization snapshots for (a) $\alpha = 0.1$ and (b) $\alpha = 0.2$. For the case of $\alpha = 0.1$, a magnetic droplet instead of circular skyrmion is formed after 10 ns. (c) The time evolution of m_z, suggesting the necessity of a larger damping constant for the generation of microwave frequency by breathing mode.

in Fig. 7(a), after 2 ns, smaller $\alpha = 0.1$ would result in magnetic droplet rather than a circular skyrmion. Fig. 7(c) is the time evolution of m_z for these two values of smaller α. For $\alpha = 0.1$, the breathing mode cannot be sustained after about 2 ns. It means that the magnetic droplet is no longer able to generate microwave frequency. On the other hand, a larger $\alpha = 0.2$ can facilitate breathing of the initial skyrmion, as reflected by the oscillation of m_z over time. We can realize from the results that a larger α is beneficial to the stability of a skyrmion in an NC-STO and to the breathing mode.

D. Tuning the external parameters

We adjust the external field strength B_{ext} between -0.3 T and $+0.3$ T, and the current density J_z between -5×10^8 A/cm^2 and $+5 \times 10^8$ A/cm^2, respectively. The $B_{ext} - J_z$ phase diagram is portrayed in Fig. 8(a). After 10 ns of simulation time, skyrmions of small and large size can be stored in an NC-STO, depending on the applied field and current density. The general trend is as follows. As B_{ext} is non-negative and J_z has a smaller magnitude, a skyrmion can remain stable in its initially small size. It means that a small J_z is unable to alter the damping torque, which helps the relaxation of magnetization. As B_{ext} is positive and $J_z \geq +2.5 \times 10^8$ A/cm^2, a spin-up state is formed. On the other hand, when B_{ext} is non-negative and $J_z \leq -1.5 \times 10^8$ A/cm^2, skyrmions of larger size can be formed. In this case, J_z is negative enough to excite magnetization dynamics. If B_{ext} is non-negative and J_z is approximately above $+2.5 \times 10^8$ A/cm^2, spin-up magnetization occurs because J_z results in a spin transfer torque that acts in the same sense as the damping torque, forcing the magnetization further toward the effective field direction.

The magnetization is different when B_{ext} is negative. In this case, the spin-down state becomes the most commonly found result for all the current densities attempted, especially when J_z is negative. As J_z is positive and its magnitude is moderate, the initial skyrmion can still be stabilized after 10 ns. But for larger magnitude of J_z, the spin-up state prevails. As a brief summary of Fig. 8(a), a skrymion can exist in an NC-STO as long J_z does not oppose B_{ext} severely.

Fig. 8(b) displays the breathing frequency of the skyrmions shown in Fig. 8(a). According to our simulations, the range of J_z that allows for frequency excitation increases with B_{ext}. When the field strength increases, the same J_z can bring about a higher operating frequency. The simulation result agrees with the experimental results of conventional STOs.[17] Besides, the breathing frequency
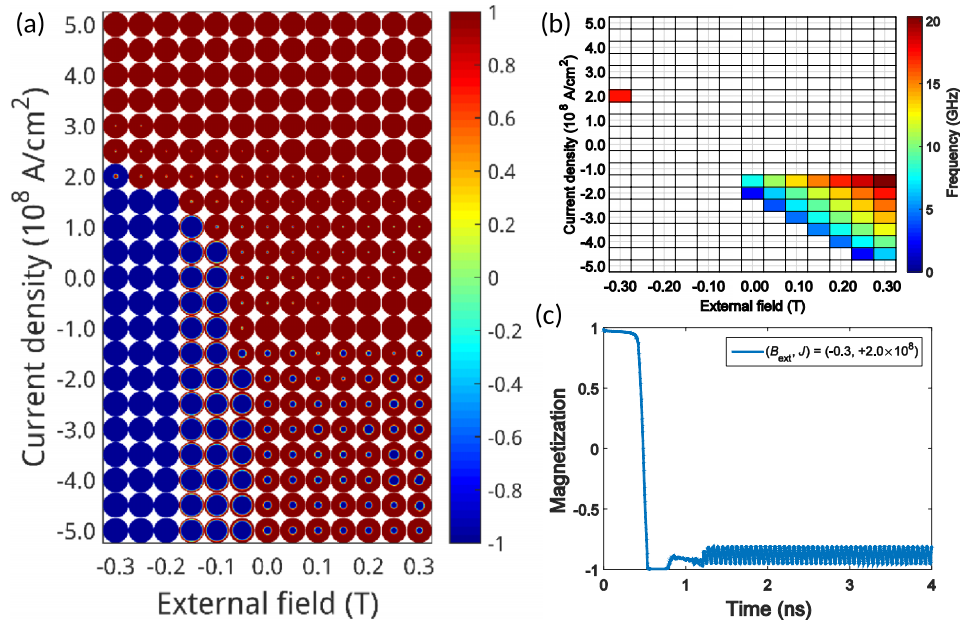

FIG. 8. (a) The $B_{ext} - J_z$ phase diagram by collocating the magnetization snapshots at 10 ns. The value of m_z is given in the color bar. (b) The main frequency of the STOs. (c) The time variation of the out-of-plane magnetization m_z of phase point $(B_{ext}, J_z) = (-0.3, +2.0 \times 10^8)$ for the first 4 ns, indicating the generation of a breathing skyrmion with reversed polarity.

increases with B_{ext} and decreases with the magnitude of J_z, same as the analytical results obtained by Hoefer *et al.*[36] The decrease in frequency with J_z is attributed to the larger domain area that requires a longer time for a complete rotation of the topological density.[37] The colors in Fig. 8(b) are more evenly spread with the variation of the applied field and current density.

While a negative B_{ext} would bring about the spin-down state in general, a breathing skyrmion with positive polarity could result at $(B_{ext}, J_z) = (-0.3, +2.0 \times 10^8)$. Fig. 8(c) gives the variation of m_z for the first 4 ns. The magnetization of the free layer follows the external field direction for the first 0.5 ns. However, it can begin to fluctuate after 1 ns, showing the generation of breathing frequency. Therefore, an external field reversed in direction may not totally destroy a skyrmion. Instead, a skyrmion having a reversed polarity can still exist in the presence of a suitable J_z.

The effect of the external field is further investigated by setting -0.3 T $\leq B_{ext} \leq +0.3$ T and $0° \leq \theta \leq 180°$. The $B_{ext} - \theta$ phase diagram just after 10 ns is shown in Fig. 9(a). We can see that a skyrmion can be stabilized as long as the angle between the external field vector $\mathbf{B}_{ext}$ and the skyrmion core magnetization $\mathbf{m}_{core}$ is obtuse, *i.e.* $\mathbf{B}_{ext} \cdot \mathbf{m}_{core} \leq 0$. The main frequency component of the breathing skyrmions is shown in Fig. 9(b), all of which are found to be fundamental frequencies. As the direction of the magnetic field tends to align with the out-of-plane direction $(\theta \to 0°)$ or $(\theta \to 180°)$, the fundamental frequency of breathing increases. Besides, with the magnetic field strength being kept constant (as shown in Fig. 9(c)), an decrease in θ leads to the blue shift of the fundamental frequency and to the declining power of higher harmonics. However, a perpendicularly out-of-plane magnetic field (*i.e.* $\theta = 0°$ or $180°$) is unable to remove the higher harmonics. When the magnetic field is directed parallel to the free layer $(\theta = 90°)$, a skyrmion can just remain in a static mode without breathing. This result indicates that the presence of an oblique magnetic field warrants breathing.
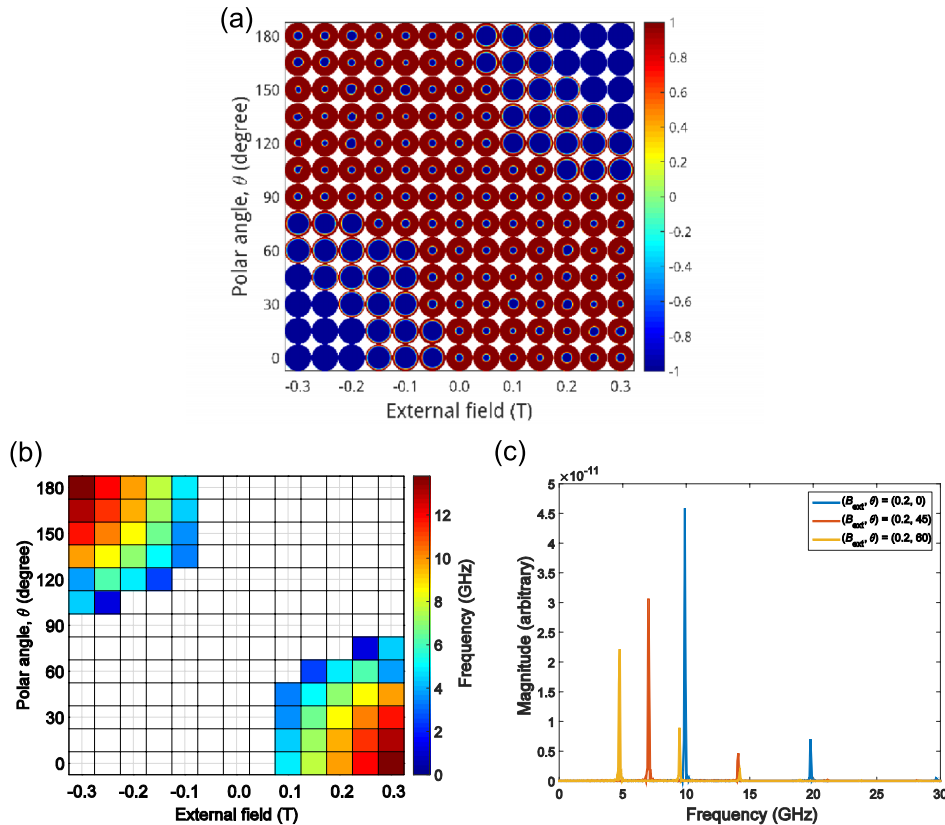

FIG. 9. (a) The $B_{ext} - \theta$ phase diagram composed of the snapshots at 10 ns. The color bar on the right shows the scale of m_z. (b) The main frequency of the STOs as the time approaches 10 ns. (c) The frequency spectra of m_z for three phase points (0.2, 0), (0.2, 45) and (0.2, 60), showing the increase in the fundamental frequency with the decrease in the magnetic field angle θ.

The $B_{ext} - \theta$ phase diagram is symmetric about the central phase point $(0, 90)$ because changing the sign of B_{ext} has the same effect of reversing the out-of-plane component of the magnetic field vector.

IV. DISCUSSION

The deviation of the polarization angle from the current-perpendicular-to-plane (CPP) configuration introduces higher harmonics of high power, making the frequency trend in Fig. 2(b) highly unpredictable. This result is drastically different from conventional NC-STOs, which can result in gradual transition of operating frequency (as shown in Fig. 2(a) of Ref. 38). Therefore, changing β is not a suitable way of stabilizing a static skyrmion.

We notice from Fig. 2(a) that the core of the resulting equilibrium skyrmions, if any, is distorted to follow that of the fixed layer after passing through a spin-polarized current. In fact, the polarization angle affects the direction of both the in-plane and field-like torques, according to Eq. (1). The complete winding of a skyrmion is then destroyed. Phase points with $\beta \leq 40°$ are clear examples of this condition. In other words, the out-of-plane polarization is crucial for the topological protection demonstrated by a skyrmion.

The wide range of the $\Lambda - \epsilon'$ phase points that allows for formation of a skyrmion is understandable. As long as the electrons can pass through the spacer, the in-plane torque can be established and then the magnetization of the free layer can be obtained.

As can be seen from Fig. 3(b), tuning these spacer parameters cannot result in a wider range of the breathing frequency. Therefore, it is better to rely on adjusting the material and external parameters in order to vary the operating frequency. The spacer can have a more lenient choice that simply allows electronic current to pass through.

The NC-STOs that can breathe at tens of GHz are found to have small M_{sat} and large A_{ex}, both of which determine the exchange field according to the equation

$$\mathbf{B}_{exch} = \frac{2A_{ex}}{M_{sat}} \Delta \mathbf{m}. \tag{4}$$

In Eq. (4), $\Delta \mathbf{m}$ is the total change in magnetization relative to the neighboring cells. It follows from our findings in Fig. 4(b) that high breathing frequency occurs at large exchange interaction. In fact, such a high frequency is commonly used in satellite communications. It is thus unsurprising that skyrmion-based NC-STOs can be applied to this area.

The possibility of producing NC-STOs at small saturation magnetization leads to a wider choice of the free layer materials other than highly ferromagnetic ones. A candidate of such materials is ferrofluids, whose M_{sat} can be as small as 32 kA/m.[39]

It is shown in the previous section that the breathing mode of a skyrmion in an NC-STO diminishes with increasing DMI. It implies that a lower DMI is preferred if one relies on the breathing mode as the source of microwave generation. In addition, the possible variation of the breathing frequency at a longer simulation time further weakens the justification of both a large DMI and a large PMA in practical applications of microwave oscillators. Accordingly, one should avoid the boundary points in the application of stable frequency generation.

Indeed, our $D_{ind} - K_u$ phase diagram has verified that a high PMA in the absence of DMI is sufficient to warrant the formation of a skyrmion,[5] whose stability is attributed to the application of a magnetic field and a spin-polarized current. However, no breathing occurs on these STOs, as reflected by the zero values on the far left column of Fig. 5(b). Therefore, a finite amount of DMI is still crucial for the frequency generation of skyrmion-based STOs.

In the case of a nanowire without application of field and current, no such variation of the skyrmion mode has been reported.[33] Further experimental investigation is thus necessary to justify the effect of the DMI on the frequency stability of the STO operation over time.

Our $d_{contact} - d_{layer}$ phase diagram in Fig. 6(a) indicates that the nanocontact diameter that can trigger breathing has a similar range (about $30 - 60$ nm in our simulation). The phase diagram also suggests that the free layer diameter does not need to be large, because it is the free layer region

underneath the nanocontact area that controls the spin wave mode. The free layer just needs to be sufficiently large to accommodate a nanocontact that can excite the desired mode of excitation.

We may analyze the breathing frequency of the $B_{ext} - J_z$ phase diagram using Eq. (1). As J_z becomes more negative, the in-plane torque pushes the free layer magnetization harder away from the fixed layer, which is along the $+z$-direction. By conservation of angular momentum, the magnetization oscillates at a lower frequency in this case. The field-like torque is more insignificant than the in-plane torque,[32] so its presence cannot alter the effect due to the in-plane torque.

The pattern of frequency generation of skyrmion-based STOs due to the application of field and current resembles the conventional STOs. It implies that the conventional approaches to controlling the operating frequency is generally applicable to skyrmion-based STOs as well.

Aligning the magnetic field toward the out-of-plane direction can inhibit the power of higher harmonics, at the expense of generating a higher fundamental frequency. It is believed that the appropriate choice of free layer materials is the best solution to a lower operating frequency while suppressing the higher harmonics.

The operating frequency is higher when the magnetic field angle approaches the out-of-plane direction, which is opposite to the case of conventional NC-STO.[2,40] At an in-plane magnetic field angle ($\theta = 90°$ in our case), only a static skyrmion can be stabilized. Such a result suggests that an in-plane magnetic field is likely to prevent breathing.

As a collective consideration of all the phase diagrams attempted, the maintenance of a static skyrmion in an STO is easier than keeping it in a breathing mode. Control of the breathing frequency is most efficiently performed by tuning the external magnetic field vector and the magnitude of the current density. For a wider range of tunable frequency (up to tens of GHz), materials with extremely low saturation magnetization, high PMA, and strong DMI can be chosen.

It is found that a larger damping parameter of $\alpha > 0.1$ for Co to generate high frequency microwave signal in the proposed NC-STO. In order to utilize such NC-STO as tunable microwave generator, the material with a smaller damping such as CoFeB thin film need to be incorporated while keeping relatively large K_u and DMI. The main results and conclusions using a small damping should remain qualitatively unchanged if we consider a soft material with smaller damping.

V. CONCLUSION

A number of feasible conditions for the stability of a skyrmion in an NC-STO have been studied. The tilting of the polarization is not beneficial to the skyrmion-based NC-STOs due to the accompanying harmonics of microwave power. Although the DMI is not a crucial factor of skyrmion stability in an NC-STO, it is prerequisite for microwave frequency generation. The nanocontact diameter seems to be a factor of the threshold current that is responsible for the breathing mode of a skyrmion. Adjustment of the breathing frequency is possible by tuning the current density and the magnetic field vector.

[1] S. I. Kiselev, J. C. Sankey, I. N. Krivorotov, N. C. Emley, R. J. Schoelkopf, R. A. Buhrman, and D. C. Ralph, "Microwave oscillations of a nanomagnet driven by a spin-polarized current," Nature **425**, 380–383 (2003).

[2] W. H. Rippard, M. R. Pufall, S. Kaka, T. J. Silva, and S. E. Russek, "Current-driven microwave dynamics in magnetic point contacts as a function of applied field angle," Phys. Rev. B **70**, 100406(R) (2004).

[3] F. Jonietz, S. Mühlbauer, C. Pfleiderer, A. Neubauer, W. Münzer, A. Bauer, T. Adams, R. Georgii, P. Böni, R. A. Duine, K. Everschor, M. Garst, and A. Rosch, "Spin transfer torques in MnSi at ultralow current densities," Science **330**, 1648 (2010).

[4] K. Everschor, M. Garst, R. A. Duine, and A. Rosch, "Current-induced rotational torques in the skyrmion lattice phase of chiral magnets," Phys. Rev. B **84**, 064401 (2011).

[5] K. Y. Guslienko, "Skyrmion state stability in magnetic nanodots with perpendicular anisotropy," IEEE Magn. Lett. **6**, 4000104 (2015).

[6] I. Dzyaloshinskii, "A thermodynamic theory of 'weak' ferromagnetism of antiferromagnetics," J. Phys. Chem. Solids **4**, 241–255 (1958).

[7] T. Moriya, "Anisotropic superexchange interaction and weak ferromagnetism," Phys. Rev. **120**, 91–98 (1960).

[8] S. Zhang, J. Wang, Q. Zheng, Q. Zhu, X. Liu, S. Chen, C. Jin, Q. Liu, C. Jia, and D. Xue, "Current-induced magnetic skyrmions oscillator," New J. Phys. **17**, 023061 (2015).

[9] Y. Zhou, C. L. Zha, S. Bonetti, J. Persson, and J. Åkerman, "Spin-torque oscillator with tilted fixed layer magnetization," Appl. Phys. Lett. **92**, 262508 (2008).

[10] Y. Zhou, H. Zhang, Y. Liu, and J. Åkerman, "Macrospin and micromagnetic studies of tilted polarizer spin-torque nano-oscillators," J. Appl. Phys. **112**, 063903 (2012).

[11] Y. Zhou, "Effect of the field-like spin torque on the switching current and switching speed of magnetic tunnel junction with perpendicularly magnetized free layers," J. Appl. Phys. **109**, 023916 (2011).

[12] Ar. Abanov and V. L. Pokrovsky, "Skyrmion in a real magnetic film," Phys. Rev. B **58**, R8889–R8892 (1998).

[13] A. S. Kirakosyan and V. L. Pokrovsky, "From bubble to Skyrmion: Dynamic transformation mediated by a strong magnetic tip," J. Magn. Magn. Mater. **305**, 413–422 (2006).

[14] J. C. Slonczewski, "Excitation of spin waves by an electric current," J. Magn. Magn. Mater. **195**, L261–L268 (1999).

[15] S. Bonetti, V. Tiberkevich, G. Consolo, G. Finocchio, P. Muduli, F. Mancoff, A. Slavin, and J. Åkerman, "Experimental evidence of self-localized and propagating spin wave modes in obliquely magnetized current-driven nanocontacts," Phys. Rev. Lett. **105**, 217204 (2010).

[16] Y. Liu, H. Li, Y. Hu, and A. Du, "Oscillation frequency of magnetic vortex induced by spin-polarized current in a confined nanocontact structure," J. Appl. Phys. **112**, 093905 (2012).

[17] W. H. Rippard, M. R. Pufall, S. Kaka, S. E. Russek, and T. J. Silva, "Direct-current induced dynamics in $Co_{90}Fe_{10}/Ni_{80}Fe_{20}$ point contacts," Phys. Rev. Lett. **92**, 027201 (2004).

[18] W. H. Rippard, M. R. Pufall, and S. E. Russek, "Comparison of frequency, linewidth, and output power in measurements of spin-transfer nanocontact oscillators," Phys. Rev. B **74**, 224409 (2006).

[19] G. Consolo, B. Azzerboni, L. Lopez-Diaz, G. Gerhart, E. Bankowski, V. Tiberkevich, and A. N. Slavin, "Micromagnetic study of the above-threshold generation regime in a spin-torque oscillator based on a magnetic nanocontact magnetized at an arbitrary angle," Phys. Rev. B **78**, 014420 (2008).

[20] G. Finocchio, O. Ozatay, L. Torres, R. A. Buhrman, D. C. Ralph, and B. Azzerboni, "Spin-torque-induced rotational dynamics of a magnetic vortex dipole," Phys. Rev. B **78**, 174408 (2008).

[21] Q. Mistral, M. van Kampen, G. Hrkac, J.-V. Kim, T. Devolder, P. Crozat, C. Chappert, L. Lagae, and T. Schrefl, "Current-driven vortex oscillations in metallic nanocontacts," Phys. Rev. Lett. **100**, 257201 (2008).

[22] T. Devolder, J.-V. Kim, M. Manfrini, W. van Roy, L. Lagae, and C. Chappert, "Vortex nucleation in spin-torque nanocontact oscillators," Appl. Phys. Lett. **97**, 072512 (2010).

[23] A. V. Khvalkovskiy, J. Grollier, N. Locatelli, Ya. V. Gorbunov, K. A. Zvezdin, and V. Cros, "Nonuniformity of a planar polarizer for spin-transfer-induced vortex oscillations at zero field," Appl. Phys. Lett. **96**, 212507 (2010).

[24] V. S. Pribiag, I. N. Krivorotov, G. D. Fuchs, P. M. Braganca, O. Ozatay, J. C. Sankey, D. C. Ralph, and R. A. Buhrman, "Magnetic vortex oscillator driven by d.c. spin-polarized current," Nature Phys. **3**, 498–503 (2007).

[25] A. Dussaux, B. Georges, J. Grollier, V. Cros, A. V. Khvalkovskiy, A. Fukushima, M. Konoto, H. Kubota, K. Yakushiji, S. Yuasa, K. A. Zvezdin, K. Ando, and A. Fert, "Large microwave generation from current-driven magnetic vortex oscillators in magnetic tunnel junctions," Nat. Commun. **1**, 1–6 (2010).

[26] A. Vansteenkiste, J. Leliaert, M. Dvornik, M. Helsen, F. Garcia-Sanchez, and B. Van Waeyenberge, "The design and verification of MuMax3," AIP Adv. **4**, 107133 (2014).

[27] J. C. Slonczewski, "Currents and torques in metallic magnetic multilayers," J. Magn. Magn. Mater. **247**, 324–338 (2002).

[28] J. Xiao, A. Zangwill, and M. D. Stiles, "Boltzmann test of Slonczewski's theory of spin-transfer torque," Phys. Rev. B **70**, 172405 (2004).

[29] A. A. Tulapurkar, Y. Suzuki, A. Fukushima, H. Kubota, H. Maehara, K. Tsunekawa, D. D. Djayaprawira, N. Watanabe, and S. Yuasa, "Spin-torque diode effect in magnetic tunnel junctions," Nature **438**, 339–342 (2005).

[30] J. Sampiao, V. Cros, S. Rohart, A. Thiaville, and A. Fert, "Nucleation, stability and current-induced motion of isolated magnetic skyrmions in nanostructures," Nature Nanotech. **8**, 839C-844 (2013).

[31] M. Mochizuki, "Spin-wave modes and their intense excitation effects in skyrmion crystals," Phys. Rev. Lett. **108**, 017601 (2012).

[32] A. Brataas, A. D. Kent, and H. Ohno, "Current-induced torques in magnetic materials," Nature Mater. **11**, 372–381 (2012).

[33] J.-W. Yoo, S.-J. Lee, J.-H. Moon, and K.-J. Lee, "Phase diagram of a single skyrmion in magnetic nanowires," IEEE Trans. Magn. **50**, 1500504 (2014).

[34] A. N. Slavin and P. Kabos, "Approximate theory of microwave generation in a current-driven magnetic nanocontact magnetized in an arbitrary direction," IEEE Trans. Magn. **41**, 1264–1273 (2005).

[35] V. Puliafito, B. Azzerboni, G. Consolo, G. Finocchio, L. Torres, and L. Lopez Diaz, "Micromagnetic modeling of nanocontact spin-torque oscillators with perpendicular anisotropy at zero bias field," IEEE Trans. Magn. **44**, 2512–2515 (2008).

[36] M. A. Hoefer, T. J. Silva, and M. W. Keller, "Theory for a dissipative droplet soliton excited by a spin torque nanocontact," Phys. Rev. B **82**, 054432 (2010).

[37] G. Finocchio, V. Puliafito, S. Komineas, L. Torres, O. Ozatay, T. Hauet, and B. Azzerboni, "Nanoscale spintronic oscillators based on the excitation of confined soliton modes," J. Appl. Phys. **114**, 163908 (2013).

[38] Y. Zhou, C. L. Zha, S. Bonetti, S. Persson, and J. Åkerman, "Microwave generation of tilted-polarizer spin torque oscillator," J. Appl. Phys. **105**, 07D116 (2009).

[39] R. Ravaud and G. Lemarquand, "Mechanical properties of a ferrofluid seal: Three-dimensional analytical study based on the coulombian model," Prog. Electromagn. Res. B **13**, 385C-407 (2009).

[40] S. Bonetti, P. Muduli, F. Mancoff, and J. Åkerman, "Spin torque oscillator frequency versus magnetic field angle: The prospect of operation beyond 65 GHz," Appl. Phys. Lett. **94**, 102507 (2009).